Arbitrary void feature control in level set topology optimization

Jikai Liu, Lin Cheng, and Albert C. To*

Department of Mechanical Engineering and Materials Science, University of Pittsburgh, Pittsburgh, Pennsylvania 15261, USA

*Corresponding author. Email: albertto@pitt.edu

Abstract

Feature-driven topology optimization has been extensively studied in the past decade, and the majority of the works have treated it as the multi-component/void layout optimization problem. A major limitation of this treatment is that the number of components/voids should be defined in advance. To overcome this limitation, this paper presents a novel void feature control method, through which the specified void feature (in any geometric form) could be well-contained by each interior void in the finalized topology design, regardless of the quantity. Numerical stability of this method is discussed and an auxiliary algorithm has been developed to enhance it. Other than that, the proposed method also serves the purpose of void length scale control, which is also a hot issue in the topology optimization field. To be specific, by tailoring the specified void feature size, the void length scale is guaranteed to be larger than that. To the authors' knowledge, the void length scale control was rarely studied under the level set framework. Through a few numerical case studies, it is proven that the void feature control method is effective while only limited compromise of the structural performance has been observed.

Keywords: Void feature control; Level set; Topology optimization; Length scale control

1. Introduction

Topology optimization has been actively investigated in the past few decades. So far, the SIMP (Solid Isotropic Material with Penalization) [1,2], ESO (Evolutionary Structural Optimization) [3], and level set [4,5] are the main topology optimization methods. These methods all have their unique characteristics and at the same time, are tightly associated. A broad range of design problems governed by different physical disciplines have been solved through these methods, i.e. solid mechanics [1,3–6], fluid dynamics [7–10], and thermal dynamics [1,11–14], etc. A few comprehensive literature surveys can be found in [15–20].

On the other hand, topology optimization is still not fully developed in several aspects, which include the feature-driven topology optimization and length scale control issue and will be highlighted in this work.

Feature-driven topology optimization is motivated by the need that engineering features are commonly-used design elements, which occasionally are forced to be preserved during freeform topology optimization process [21–23]. Hence, feature-driven topology optimization, so far, has mainly been treated as a multi-component/void layout optimization problem, where the components/voids only have DoF (degrees of freedom) of movement, rotation, and scaling. A major limitation is that the component/void feature quantity is pre-determined but cannot be dynamically changed during solution of

the optimization problem. In some other works [24,25], approaches have been developed to create void features to replace freeform topological changes. Even though they are not mature enough, these methods have the potential to facilitate post-treatment of CAD modeling and editing, and at the same time, enhance the manufacturability.

Length scale control is more tightly related to design for manufacturability issues [18,26]. As well known, small voids are non-manufacturable because of the cutting tool access difficulty, and small components have the risk of breakage during the machining process. Even for additive manufacturing process, voids and components that are too small are non-preferable design features given the poor build quality and possible failures. The length scale control issue has been extensively tackled based on both SIMP [27–36] and level set [37–43] methods. In this work, we have the specific interest in the level set method, and thus, the length scale control techniques under the level set framework are highlighted. From the authors' perspective, level set method has its unique characteristic in length scale control, because of the signed distance information, which makes it trivial to timely evaluate the length scales. Therefore, we have witnessed a series of works producing strip-like topology design solutions with well constrained length scales [37–39,42,44]. On the other hand, the void length scale control has rarely been implemented based on the level set method, except the authors' recent work [43].

In summary, both feature-driven topology optimization and length scale control have been extensively studied, but there is still room for further development. Hence, we contribute a novel void feature control method, which can be utilized to control the length scale of void. To be specific, constraints have been developed to realize the void feature control, which realizes the effect that the specific void feature (in any geometric form) is well-contained by each of the interior voids in the final topological design. An auxiliary algorithm has been developed based on our previous work [43] to enhance the numerical implementation stability. This method characterizes in the aspect that, the quantity and positions of the void features are not required to be pre-specified, while this information of the void features is tightly bonded to the topology evolution history and determined by the finalized topology structure. At the same time, the void length scale is constrained to be larger than that of the selected void feature size. More details will be presented in the later sections.

2. Literature survey

2.1 Feature-driven topology optimization

Feature control in topology optimization originates from the perimeter control, where the number and shape of the void features are significantly influenced by the assigned perimeter upper limit; and the specific perimeter control methods have been developed under different topology optimization frameworks, e.g., [45] for density method, [4] for level set method, and [46,47] for phase field method. Constraining the perimeter indirectly reduces the number of void features remaining in the topology optimization result and vanishes the high-curvature areas; and its concept contributed to the further development of TO technology.

On the other hand, the geometric feature, e.g. moving components, is not directly involved if only considering perimeter control. Hence, later, topology optimization involving specific geometric feature control are focused and several effective methods have been developed.

Under the SIMP framework, early efforts mainly focused on concurrent multi-component layout and support structure optimization [21,23], which optimized the components' positions through parametric sensitivity analysis and support structure through SIMP method. The multi-component overlap was prevented through the so-called finite circle method [23]. However, this approach has the limitation that the component-support interface areas were repeatedly re-meshed because of the moving components. To fix this issue, improvements were made in their later works [48,49] and [50], by adopting the level set based component representation and the X-FEM which altogether eliminates the repeated re-meshing. Recently, several modified non-overlap constraints have been developed, including the modified finite circle method through KS function-based constraint aggregation [51], the structural skeleton-based constraint [52], and the virtual boundary offset-based constraint [53].

In some recent works under the SIMP framework, Almeida et al. [54] proposed the inverse projection scheme to control the length scale of the voids (containing a circular void feature in prescribed size). Ha et al. [55] and Guest [56] developed a Heaviside projection based component layout design method which enabled the creation of small components and realized the non-overlap control. Recently, Norato et al. [57] inherited the idea from [58] by filling the design domain completely with components. A geometry projection method was developed to optimize the component feature parameters.

Feature-driven topology optimization under the level set framework can trace back to [25,59,60]. They used parametric level set functions to represent the void features, which were combined through R-functions to form complex CSG (Constructive Solid Geometry) models. Parametric sensitivity analysis was performed to update the void features. Gopalakrishn and Suresh [61] developed the feature-specific topological derivative algorithm to introduce both internal and boundary features into the 2D design domain. Zhou and Wang [62] manipulated the geometric features in a different way that, boundary velocity fields of the geometric features were regulated via least squares fitting to reserve the shape characteristics; by doing so, they realized the concurrent feature control and freeform support structure design. This least squares fitting idea was inherited by [24] to generate void features through a boundary-based approach, where the finalized topology design can be physically produced through 2.5D machining. Recently, Guo et al. [58] and Zhang et al. [63] conducted topology optimization based on the Moving Morphable Components (MMC). The pre-specified MMCs were optimized of the DoF including movement, rotation, and scaling, which finally produces the pure component feature-based design solution. Later, this method was extended to cover curved components [64]. Zhou [65] modified the method by enabling the complex mechanical parts as the moving components.

In summary, the feature-driven topology optimization is still immature, especially given that quantity of the components/void features has to be pre-determined and dynamic change during the optimization process is near impossible. Hence, the void feature control method proposed in this work addresses this issue.

2.2 Length scale control

Under the SIMP framework, Poulsen [30] developed the local integral constraints to address the minimum length scale control of both the component and void phases, which principally checked the monotonic density variations. Guest et al. [29] developed a circular density filter, which coupled with the Heaviside function, realized the minimum component length scale control. Later, in order to realize the length scale control of both the component and void phases, a modified double Heaviside projection was

developed [27]. Sigmund [33] developed a series of morphology-based density filters which realized both the single-phase and double-phase minimum length scale controls. However, as mentioned in the same paper, the sensitivity analysis of the double-phase minimum length scale control is too costly, which is even compatible to the finite element analysis (FEA). Based on the erode and dilate operations, a robust topology optimization method [31,32,34] was developed, in which multiple design realizations were evaluated while the worst case was optimized. The double-phase minimum length scale control can be achieved in case that the multiple realizations keep a consistent topology [31,34,36]. A limitation of this method is that multiple FEAs are performed in each optimization loop.

Other than the minimum length scale control, Guest et al. [28] realized the maximum component length scale control by restricting any circular areas in diameter of the maximum length scale not fully filled. Zhang et al. [35] realized the simultaneous maximum and minimum component length scale control through the structural skeleton based constraints.

Level set method is also effective in length scale control, especially given the signed distance information, which greatly facilitates the length scale measure and control. Chen et al. [38] and Luo et al. [41] employed a quadratic energy functional as part of the objective function, which successfully realized the strip-like topology design with controlled thickness. Liu et al. [40] developed a simplified thickness control functional to realize the close-to-uniform rib thickness distribution. Guo et al. [39] realized the concurrent maximum and minimum component length control through the structural skeleton based constraints which is similar to the algorithm in [35] in principle. The signed distance information facilitated the narrow-band structural skeleton extraction and related global constraints were constructed to restrict the component length scales. Xia and Shi [42] modified the structural skeleton based method. The trimmed structural skeleton and the concept of maximal inscribable ball were employed to evaluate the length scale. Discrete point-based structural skeleton was extracted instead of a narrow band which facilitated the distance evaluation from skeleton. In this way, the length scale constraints were directly applied to the structural boundary points. Allaire et al. [37] explored the length scale control in depth under different schemes of maximum length scale only, minimum length scale only, and simultaneous control. Wang et al. [44] realized the component length scale control through proposing and addressing the contour-offset based constraints. Very recently, Liu et al. [43] proposed the minimum void length scale control method which constrained the void length scales by double lower bounds, so that the topology design can be milled by a rough-to-finish process. To the best of the authors' knowledge, this is the only work conducted so far to control the void length scale under the level set framework.

Literature surveys about the length scale control can be found in [18,26].

In summary, a variety of length scale control methods have been developed subject to different length scale control scenarios. Under the level set framework, focuses have only been put on the component length scale control, while the void length scale control was rarely explored, except the authors' recent work [43]. Therefore, the void feature control method developed in this paper serves the purpose of void length scale control, by forcing the interior voids containing the specific void features.

3. Void feature control

The purpose of void feature control is to guarantee that each of the interior voids in the finalized topology design contains a pre-specified void feature. An instance is demonstrated in Fig. 1, where each interior void contains a circular void feature. It is worth noticing that, only the interior voids are controlled but not the boundary voids.

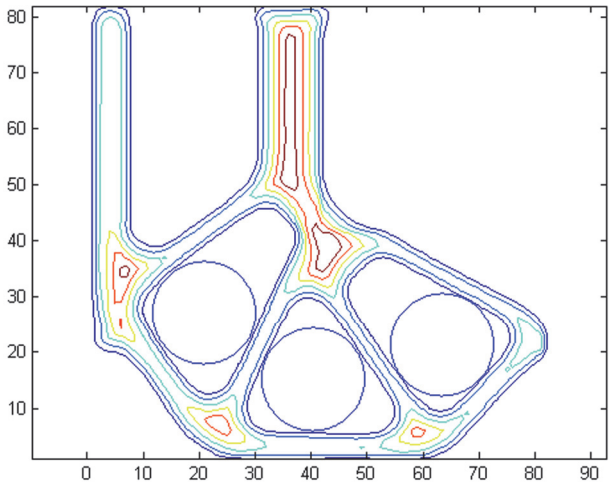

Figure 1. L-bracket design subjected to the circular void feature control

To realize the void feature control, related technical details will be presented in the rest of this section.

3.1 Level set representation of the void features

Level set function, $\Phi(\boldsymbol{X})$: $R^n \longmapsto R$, represents any structure in the implicit form, as:

$$\begin{cases} \Phi(\boldsymbol{X}) > 0, & \boldsymbol{X} \in \Omega / \partial\Omega \\ \Phi(\boldsymbol{X}) = 0, & \boldsymbol{X} \in \partial\Omega \\ \Phi(\boldsymbol{X}) < 0, & \boldsymbol{X} \in D/\Omega \end{cases} \tag{1}$$

where Ω represents the material domain, D indicates the entire design domain, and thus D/Ω represents the void.

First, individual void features can be represented by parametric level set functions. For instance, a circular void feature can be modeled by:

$$\Phi_f(\boldsymbol{X}) = sqrt((x - x_0)^2 + (y - y_0)^2) - R_c \tag{2}$$

and a square void feature by:

$$\Phi_f(\boldsymbol{X}) = -min\{\frac{H_s}{2} - (x - x_0), \frac{H_s}{2} + (x - x_0), \frac{H_s}{2} - (y - y_0), \frac{H_s}{2} + (y - y_0)\} \tag{3}$$

in which (x_0, y_0) is the feature primitive center coordinates; R_c is the circle radius and H_s is the square length.

3.2 Constraint for the void feature control

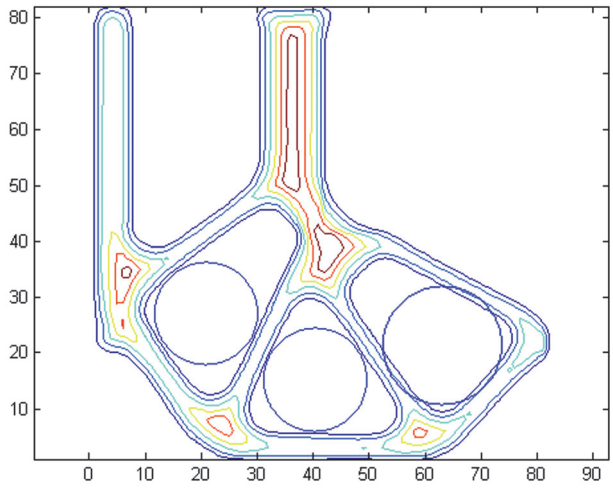

Figure 2. Violation of the void feature control

Figure 2 demonstrates an example of the void feature control violation, where we can see that the circle on the right-side intersects the structural boundary. This means that this circular void feature is not well contained by the related interior void. In order to prevent this type of violation, the void feature control constraint is developed; see Eq. (4), and later will be embedded into the optimization problem formulation.

$$\sum_{i=1}^{n} \int_{D} H\left(-\Phi_{f_i}(\boldsymbol{X})\right) * H\big(\Phi(\boldsymbol{X})\big) d\Omega \leq 0 \tag{4}$$

where n represents the number of interior voids, and $H(\quad)$ is the Heaviside function which is applied to realize the domain integration.

3.3 Identification of the interior voids

In order to properly apply the constraints, it is critical to properly identify interior voids during the optimization process. The identified n value is going to change dynamically as the topology evolves.

Generally, the level set field satisfies the signed distance regulation through the solution of Eq. (5), through which the absolute level set value at any point represents its shortest distance to the structural boundary and the sign indicates the point to be either solid (> 0), or void (< 0).

$$|\nabla\Phi(\boldsymbol{X})| = 1 \tag{5}$$

Referring to the signed distance information, the peak point concept is proposed. To be specific, we define the i^{th} interior void as ${\Omega^v}_i$ and its boundary as $\partial{\Omega^v}_i$. Peak point of the i^{th} interior void is represented by ${P^v}_i$, which is defined as: $\{\overline{\boldsymbol{X}} = \boldsymbol{X}({P^v}_i) | \Phi(\overline{\boldsymbol{X}}) < \Phi(\boldsymbol{X}), for\ any\ \boldsymbol{X} \in {\Omega^v}_i\}$. The j^{th} boundary void is represented by ${\Omega^{bv}}_j$ and its boundary by $\partial{\Omega^{bv}}_j$. Peak point of the j^{th} boundary void is represented by ${P^{bv}}_i$, which is defined as: $\{\overline{\boldsymbol{X}} = \boldsymbol{X}({P^{bv}}_j) | \Phi(\overline{\boldsymbol{X}}) < \Phi(\boldsymbol{X}), for\ any\ \boldsymbol{X} \in {\Omega^{bv}}_j\}$.

Noted that the signed distance regulation $|\nabla\Phi(\boldsymbol{X})| = 1$ is not true for points that are equidistant from at least two points on the interface. Therefore, $|\nabla\Phi(\boldsymbol{X})| = 1$ does not hold at the peak point. This is

commonly the case in level set topology optimization because only the signed distance information within a narrow band around the interface is used for design update.

The quick two-dimensional search is conducted and the peak points should satisfy the constraints in Eq. (6).

$$\begin{cases} \Phi_{k,l} - \Phi_{k-1,l} \leq 0 \\ \Phi_{k,l} - \Phi_{k+1,l} \leq 0 \\ \Phi_{k,l} - \Phi_{k,l-1} \leq 0 \\ \Phi_{k,l} - \Phi_{k,l+1} \leq 0 \end{cases} \tag{6}$$

Two situations may be encountered: The peak point ${P^v}_i$ is located inside the design domain or at the boundary. Only the former indicates the peak point of an interior void, while the latter means the peak point of a boundary void, which will not be further processed.

Note that the voids are identified through finding the peak points, and at the same time, the boundary voids are filtered by analyzing the peak point positions. In addition, the peak point concept also facilitates the spatial position search of the candidate void features; see the later Eq. (7), and will be used by the auxiliary algorithm; see the later Section 6.

3.4 Identification of the void feature parameters

So far, both the void feature control constraint and interior voids have been identified. In order to properly apply the constraints to each of the identified interior voids, parameters of each void feature should be decided as well, by referring to Eq. (4). This can be fulfilled by solving the simple optimization problem as presented in Eq. (7):

$$\begin{gathered} for\ the\ i^{th}\ interior\ void \\ find\ the\ center\ position\ (x,y)\ and\ orientation(\theta)\ of\ the\ included\ void\ feature, \\ which\ satisfies: \\ min.\ \int_D H\left(-\Phi_{f_i}(\boldsymbol{X})\right) * H\big(\Phi(\boldsymbol{X})\big) d\Omega \end{gathered} \tag{7}$$

The principle of Eq. (7) is to find the location and orientation of the included void feature, which to the lowest degree affects the structural mechanical performance. Besides, sizing parameters of the void feature is not treated as optimization variables. It is also worth noticing that, the search starts by overlapping the feature center position with the related peak point, in order to make the search process robust.

4. Optimization problem and its solution

A typical compliance minimization topology optimization problem subject to the void feature control is formulated in Eq. (8). The structural compliance is to be minimized subject to the material volume fraction constraint.

$$
\begin{aligned}
Min. \quad & J(\boldsymbol{u},\Phi) = \int_D \frac{1}{2}\boldsymbol{D}\boldsymbol{e}(\boldsymbol{u})\boldsymbol{e}(\boldsymbol{u})H(\Phi)d\Omega \\
s.t. \quad & a(\boldsymbol{u},\boldsymbol{v},\Phi) = l(\boldsymbol{v},\Phi), \forall \boldsymbol{v} \in U_{ad} \\
& \int_D H(\Phi)d\Omega \le V_{max} \\
Line\ 4: \quad & \sum_{i=1}^{n}\int_D H\left(-\Phi_{f_i}(\boldsymbol{X})\right) * H\big(\Phi(\boldsymbol{X})\big)d\Omega < 0 \\
& a(\boldsymbol{u},\boldsymbol{v},\Phi) = \int_D \boldsymbol{D}\boldsymbol{e}(\boldsymbol{u})\boldsymbol{e}(\boldsymbol{v})H(\Phi)d\Omega \\
& l(\boldsymbol{v},\Phi) = \int_D \boldsymbol{p}\boldsymbol{v}H(\Phi)d\Omega + \int_D \boldsymbol{\tau}\boldsymbol{v}\delta(\Phi)|\nabla\Phi|d\Omega
\end{aligned}
\tag{8}
$$

in which $a(\boldsymbol{u},\boldsymbol{v},\Phi)$ is the energy bilinear form and $l(\boldsymbol{v},\Phi)$ is the load linear form; $\boldsymbol{u}$ is the deformation vector, $\boldsymbol{v}$ is the test vector, and $U_{ad} = \{\boldsymbol{v} \in H^1(\Omega)^d | \boldsymbol{v} = 0\ on\ \Gamma_D\}$ is the space of kinematically admissible displacement field; $\boldsymbol{D}$ is the elasticity tensor and $\boldsymbol{e}(\boldsymbol{u})$ is the strain. V_{max} is the upper bound of the material volume. $\delta(\ \ )$ is Dirac Delta function, which is applied to realize the boundary integration. It is worth noticing that, line 1-3 and line 5-6 together form the typical compliance minimization problem under the level set framework. For more details, interested readers can refer to [5,38,66].

Other than that, line 4 is the newly propose void feature control constraints, which has been discussed in the last section.

About solution of this problem, the Augmented Lagrange Multiplier method is employed and the adjoint sensitivity analysis is performed. Typically, if only the compliance-minimization problem is considered but not the void feature control, the sensitivity result is well known as presented in Eq. (9) [5].

$$
\begin{aligned}
L' &= \int_D R\delta(\Phi)V_n|\nabla\Phi|d\Omega \\
R &= -\boldsymbol{D}\boldsymbol{e}(\boldsymbol{u})\boldsymbol{e}(\boldsymbol{u}) + \lambda \\
V_n &= -R
\end{aligned}
\tag{9}
$$

where λ is the Lagrange multiplier for the material volume fraction constraint.

If the void feature control constraint is considered simultaneously, the sensitivity result becomes:

$$L' = \int_D \overline{R}\delta(\Phi)\overline{V_n}|\nabla\Phi|d\Omega$$

$$\overline{R} = -\boldsymbol{D}\boldsymbol{e}(\boldsymbol{u})\boldsymbol{e}(\boldsymbol{u}) + \lambda + \overline{\lambda}\sum_{i=1}^{n} H\left(-\Phi_{f_i}(\boldsymbol{X})\right) \tag{10}$$

$$\overline{V_n} = -\overline{R}$$

It is worth noticing that, $\Phi_{f_i}(\boldsymbol{X})$ has been identified through solving Eq. (7). Hence, the void feature parameters would not be treated as variables when solving the optimization problem.

Based on the sensitivity result, the Hamilton-Jacobi equation is solved through the finite difference upwind scheme [67] to update the level set function.

In summary, the work flow to solve the optimization problem is presented below:

Step 1: Initialize the problem setup;

Step 2: Perform finite element analysis to calculate the state variables;

Step 3: Identify the quantity and peak point positions of the interior voids by solving Eq. (6), and determine the position and orientation of the void features by solving Eq. (7);

Step 4: Calculate the sensitivity result for design update;

Step 5: Check convergence. If yes, end the optimization process; if not, update the level set function and repeat Step 2-5.

5. Numerical Examples

In this section, a few numerical examples will be studied to prove the effectiveness of the proposed void feature control method.

For all the numerical examples, the finite element analysis (FEA) is performed based on the fixed quadrilateral mesh and the artificial weak material is employed for voids in order to avoid the stiffness matrix singularity, which is:

$$\boldsymbol{D}_v = 10^{-3}\boldsymbol{D} \tag{11}$$

where $\boldsymbol{D}_v$ is the elasticity tensor of the void.

The volume constraint is addressed by the Augmented Lagrange multiplier, as presented in Eq. (12).

$$\lambda_{k+1} = \lambda_k + \mu_k\left(\int_D H(\Phi)d\Omega - V_{max}\right)$$
$$\mu_{k+1} = \alpha\mu_k \ \ where\ 0 < \alpha < 1 \tag{12}$$

where μ is the penalization factor and α is its adjustment parameter.

5.1 Michell structure problem

First, the Michell structure problem is studied. The boundary condition is shown in Fig. 3, where the two bottom corners are fixed and a unit force is loaded at the bottom center. The objective is to minimize the structural compliance under the maximum material volume fraction of 0.3. The solid material employs the Young's Modulus of 1.3 and the Poisson's ratio of 0.4 by assumption.

Different types of void features are involved in the numerical examples. Figure 4 demonstrates the optimization results with the different-sized circular void features; Figure 5 shows the optimization results with the different-sized square void features with only the freedom of movement; and Figure 6 presents the optimization results with the different-sized rectangle void features with DoF of both movement and rotation. The optimization result without void feature control is demonstrated in Fig. 7.

In summary of these numerical examples, it is observed that, (i) the void features are well contained by the void areas, regardless of the specified feature type; and (ii) the design optimality is sacrificed by imposing the void feature control, and generally, a larger void feature would cause more optimality loss.

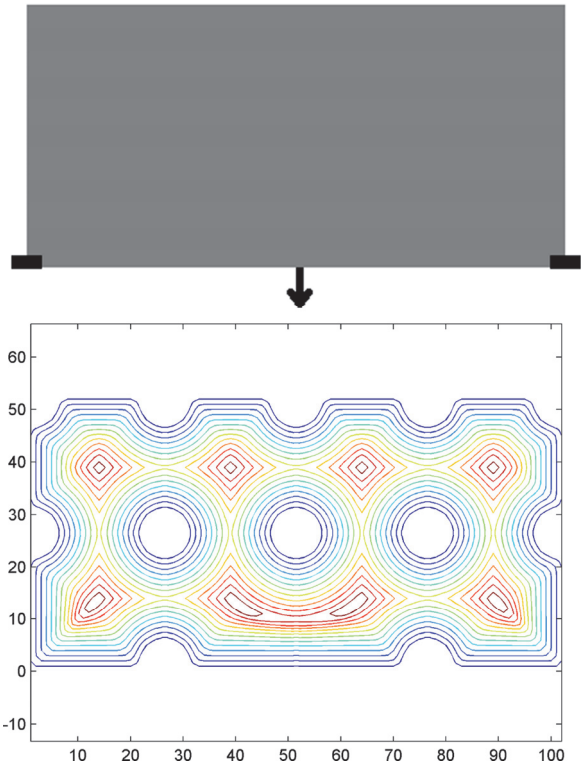

Figure 3. The Michell structure problem (100*50)

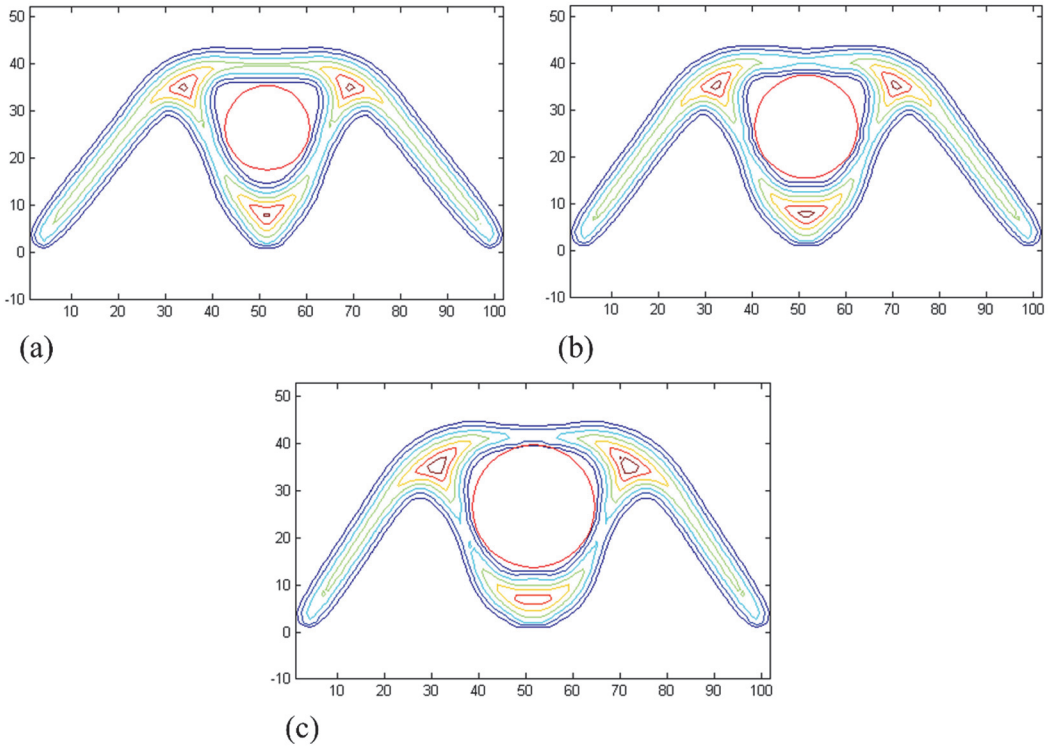

Figure 4. Optimization results with the different-sized circule void features (a) Circular void feature of R=9 (compliance = 8.93); (b) Circular void feature of R=11 (compliance = 9.37); (c) Circular void feature of R=13 (compliance = 10.22)

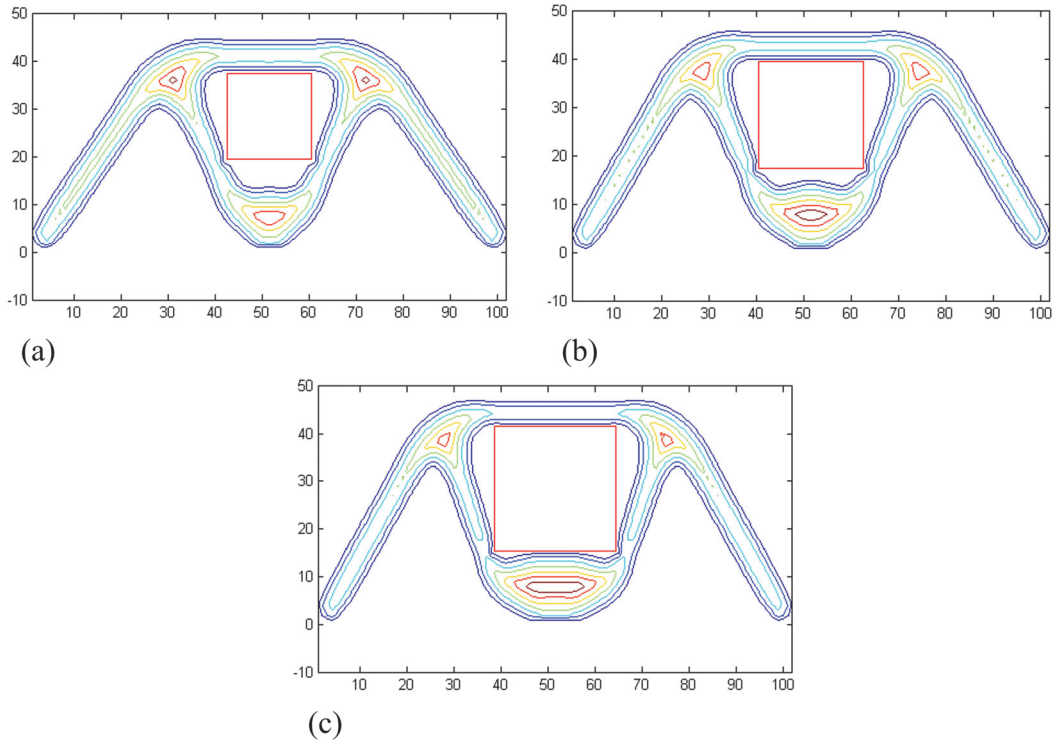

Figure 5. Optimization results with the different-sized square void features (a) Square void feature of L=18 (compliance = 9.25); (b) Square void feature of L=22 (compliance = 10.28); (c) Square void feature of L=26 (compliance = 11.45)

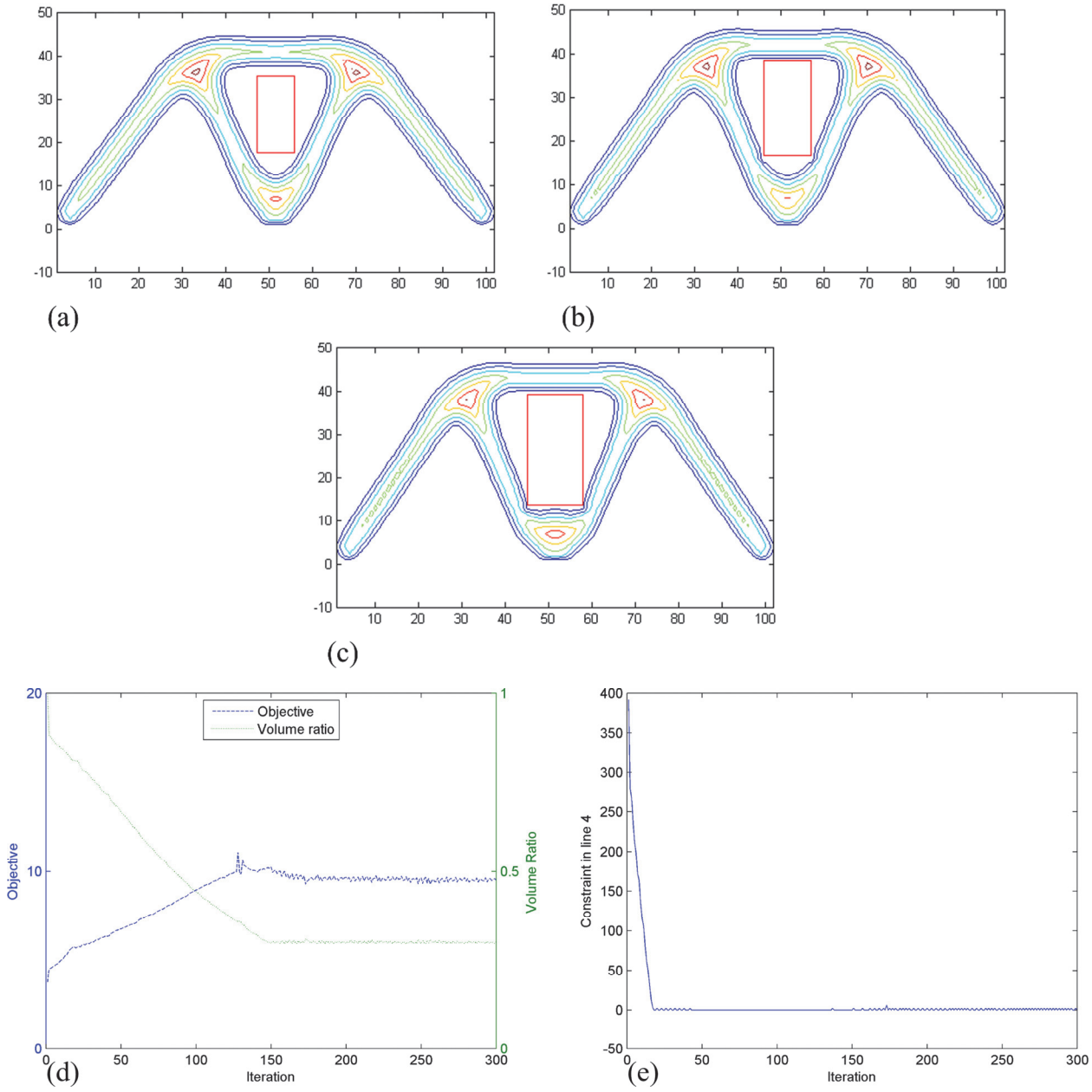

Figure 6. Optimization results with the different-sized rectangle void features (a) Rectangle void feature of L=18 and H=8 (compliance = 8.96); (b) Rectangle void feature of L=22 and H=10 (compliance = 9.03); (c) Rectangle void feature of L=26 and H=12 (compliance = 9.42); (d) Convergence history of the objective function and material volume fraction for (c); (e) Convergence history of the "line 4 constraint" for (c)

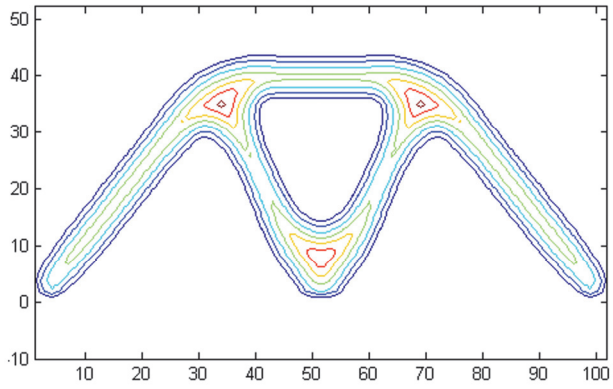

Figure 7. Optimization result without void feature control (compliance = 8.77)

5.2 L-bracket problem

The boundary condition of the L-bracket problem is shown in Fig. 8. The objective is still to minimize the structural compliance subjected to the maximum material volume fraction of 0.4. The solid material employs the Young's Modulus of 1.3 and Poisson ratio of 0.4.

Two types of void features are studied in the numerical examples. Figure 9 demonstrates the optimization results with the different-sized circular void features; Figure 10 shows the optimization results with the different-sized rectangle void features with DoF of both movement and rotation. Through the numerical studies, similar conclusions can be drawn as compared to the Michell structure example. It is worth noticing that, occasionally, minor violations can be found in the numerical examples, because the staggered boundary contour is smoothed.

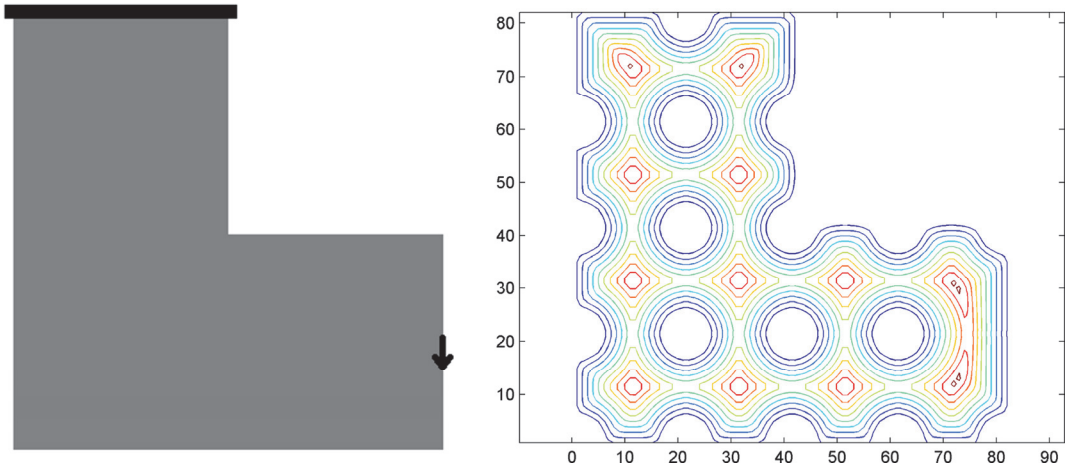

Figure 8. The L-bracket structure problem (80*80)

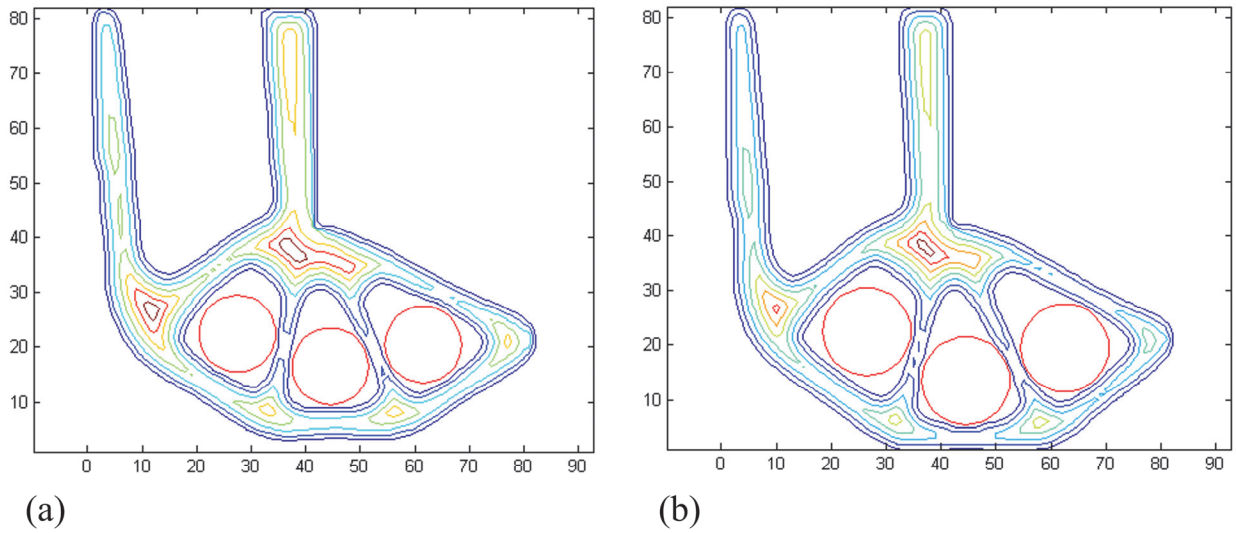

Figure 9. Optimization results with the different-sized circular void features (a) Circular void feature of R=7 (compliance = 71.00); (b) Circular void feature of R=8 (compliance = 71.39)

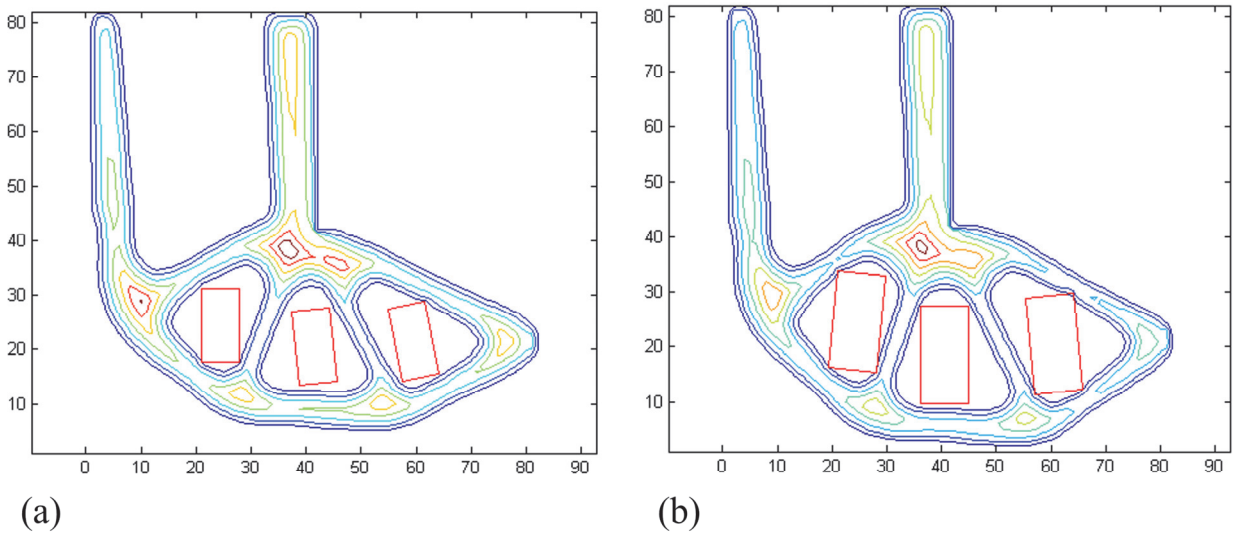

Figure 10. Optimization results with the different-sized rectangular void features (a) Rectangular void feature of L=14 and H=6 (compliance = 70.11); (b) Rectangular void feature of L=18 and H=8 (compliance = 70.26)

On the other hand, given the rectangle void feature control, numerical instability appears when we further increase the feature size. See Fig. 11 for an example. This problem arises in the case that, the candidate void feature size is much larger than the related interior void area, which causes the void feature simultaneously occupying two disconnected void areas. In such a situation, the solid area connecting the two separate voids will shrink while the void feature control constraint can never be satisfied.

A solution has been proposed to address this issue, which is demonstrated in the next section.

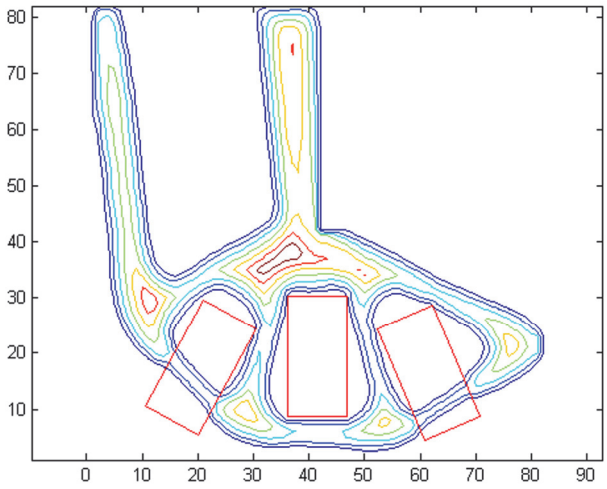

Figure 11. An example which fails of convergence (L=22 and H=10)

6. The modified problem formulation and solution

To address the stability issue, an auxiliary step is recommended before applying the void feature control constraints, and the optimization problem is expanded into two consecutive sub-problems.

Specifically, the auxiliary step is conducted to enlarge the void areas, and as discussed in the last section, the stability issue can be addressed if the void areas are sufficiently large as compared to the specified void feature size.

6.1 The auxiliary algorithm

The auxiliary algorithm is formulated below:

$$
\begin{aligned}
Min. \quad & J(\boldsymbol{u},\Phi) = \int_D \frac{1}{2}\boldsymbol{De}(\boldsymbol{u})\boldsymbol{e}(\boldsymbol{u})H(\Phi)d\Omega \\
s.t. \quad & a(\boldsymbol{u},\boldsymbol{v},\Phi) = l(\boldsymbol{v},\Phi), \forall \boldsymbol{v} \in U_{ad} \\
& \int_D H(\Phi)d\Omega \le V_{max} \\
Line\ 4: \quad & \Phi({P^v}_i) \le -K_1, \qquad i = 1,2,\dots,n
\end{aligned}
\tag{13}
$$

$$
a(\boldsymbol{u},\boldsymbol{v},\Phi) = \int_D \boldsymbol{De}(\boldsymbol{u})\boldsymbol{e}(\boldsymbol{v})H(\Phi)d\Omega
$$

$$
l(\boldsymbol{v},\Phi) = \int_D \boldsymbol{pv}H(\Phi)d\Omega + \int_D \boldsymbol{\tau v}\delta(\Phi)|\nabla\Phi|d\Omega
$$

In this problem formulation, the line 4 is newly added as compared to the conventional compliance minimization problem. It constrains the level set value at the peak point smaller than the threshold value.

The peak point identification was earlier introduced in sub-section 3.3. If the peak point level set value is smaller than $-K_1$, a circle of radius K_1 (positive) can be well contained by the related interior void. Therefore, by properly setting the K_1 value, the interior void area is enlarged to ensure the stable convergence of the following void feature-constrained optimization problem.

About solution of this constraint, it is not directly solvable because the derived sensitivity result is a local velocity located at the peak point inside the void, which cannot be utilized to update the zero-value level set contour. Therefore, we switch it into another approximated form as demonstrated in Eq. (14).

$$V_n(\boldsymbol{X}) = -\lambda_i, \qquad \boldsymbol{X} \in \partial\Omega^v{}_i$$
$$\lambda_i{}^{k+1} = \max(\lambda_i{}^k + \frac{1}{\mu_i}(\Phi(P^v{}_i) + K_1), 0) \tag{14}$$

By utilizing Eq. (14), the entire boundary of the constraint-violating void will uniformly expand. It has been numerically proven in our recent publication [43] that, this approximated solution could effectively enlarge the void areas while not evidently affect the proper convergence.

To implement Eq. (14), the main job is to identify the mapping relationship between the peak points and the related boundary points, because the peak point and the boundary points belonging to the same void should be clustered to facilitate the later sensitivity analysis. The distance could be a direct measure, because in general, the boundary point and its closest peak point belong to the same void. However, directly applying the distance measure would cause mapping errors; see Fig. 12. The green-color point at the boundary is closer to the peak point of the left void but in fact, it belongs to the structural boundary of right void. Therefore, mapping based on the simple distance measure is not always reliable.

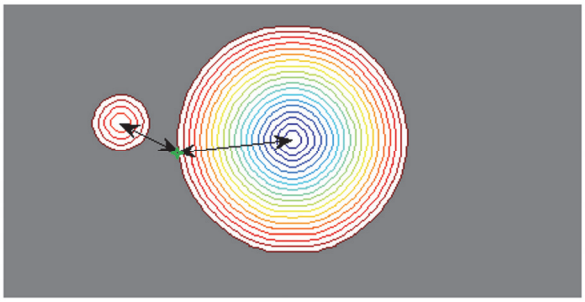

Figure 12. Incorrect mapping based on the distance standard [43]

To fix this problem, a directional distance measure is proposed, as demonstrated in Eq. (7).

$$for\ any\ boundary\ point\ \underline{\boldsymbol{X}}$$
$$find\ the\ peak\ point\ P^v{}_i, which\ satisfies:$$
$$min.\ \ f \cdot \left|\boldsymbol{X}(P^v{}_i) - \underline{\boldsymbol{X}}\right|,\ \ i = 1,2\ldots \tag{15}$$
$$\begin{cases} f = 1, \ if\ \left(\boldsymbol{X}(P^v{}_i) - \underline{\boldsymbol{X}}\right) \cdot \boldsymbol{n}\left(\underline{\boldsymbol{X}}\right) > 0 \\ f = +\infty, \ if\ \left(\boldsymbol{X}(P^v{}_i) - \underline{\boldsymbol{X}}\right) \cdot \boldsymbol{n}\left(\underline{\boldsymbol{X}}\right) \leq 0 \end{cases}$$

$$\boldsymbol{n}(\underline{\boldsymbol{X}}) = -\frac{\nabla\Phi(\underline{\boldsymbol{X}})}{|\nabla\Phi(\underline{\boldsymbol{X}})|}$$

Through Eq. (15), a correct mapping can be established in the case that the voids do not employ very irregular shapes. In addition, a small batch of mis-mapping would not affect the overall convergence.

So far, the auxiliary algorithm has been fully explained, and numerical examples will be studied to show its effectiveness.

6.2. Numerical examples

The L-bracket problem is further studied with the enhanced algorithm. The optimization results are demonstrated in Fig. 13.

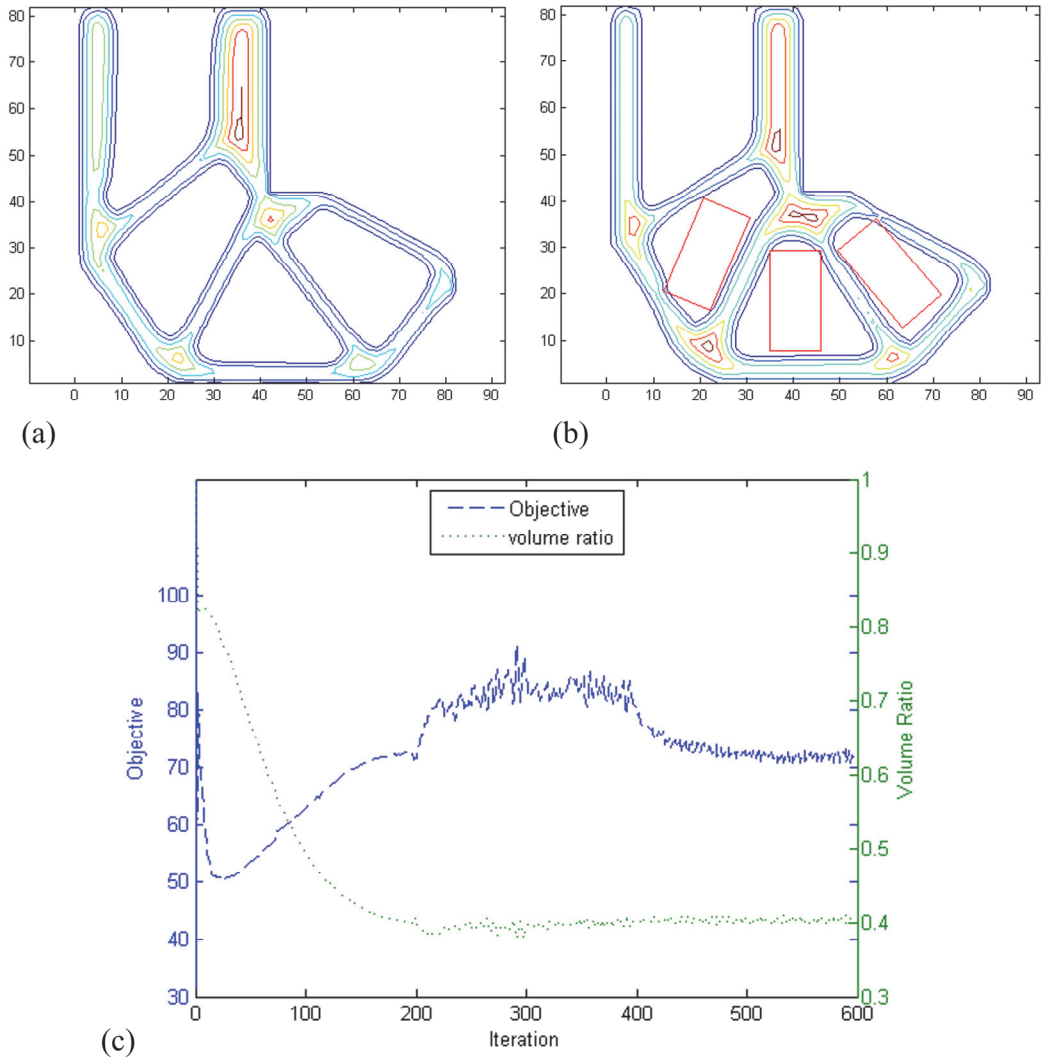

Figure 13. The modified optimization result subjected to the rectangle void feature control of size L=22 and H=10 (compliance = 72.35) (a) Optimization result of the auxiliary algorithm ($K_1 = 9.5$); (b) The final optimization result; (c) The overall convergence history

Then, the cantilever structure problem is studied subjected to the cross void feature control. As shown in Fig. 14, the left side edge is fixed and a vertical unit force is loaded at the middle of the right edge. The objective is to minimize the structural compliance under the maximum material volume fraction of 0.5. The same material properties used by the previous examples are employed.

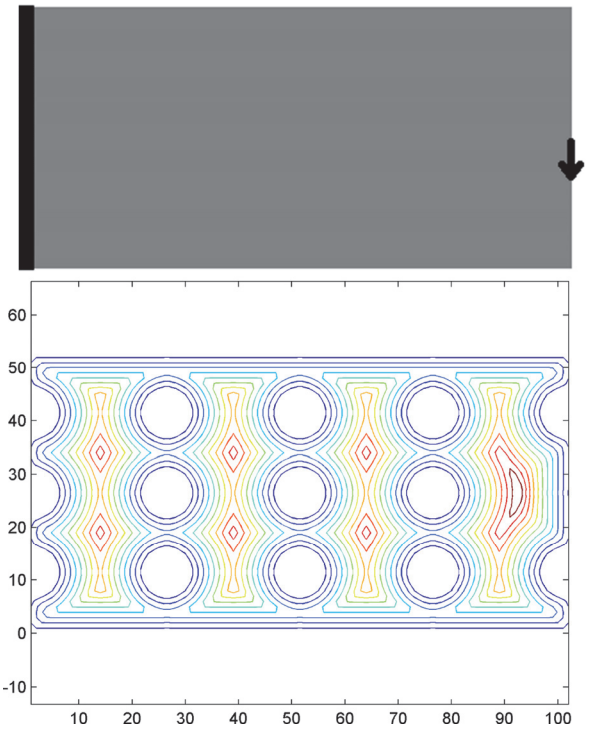

Figure 14. The cantilever structure problem (100*50)

The intermediate and final optimization results subjected to different cross void feature sizes are demonstrated in Fig. (15-17). It is interesting to find out that, the optimized results do not keep a consistent topology structure, and the primary topology structure (see Fig. 15) could be changed either during the auxiliary optimization process (see Fig. 16), or during the void feature constrained optimization process (see Fig. 17).

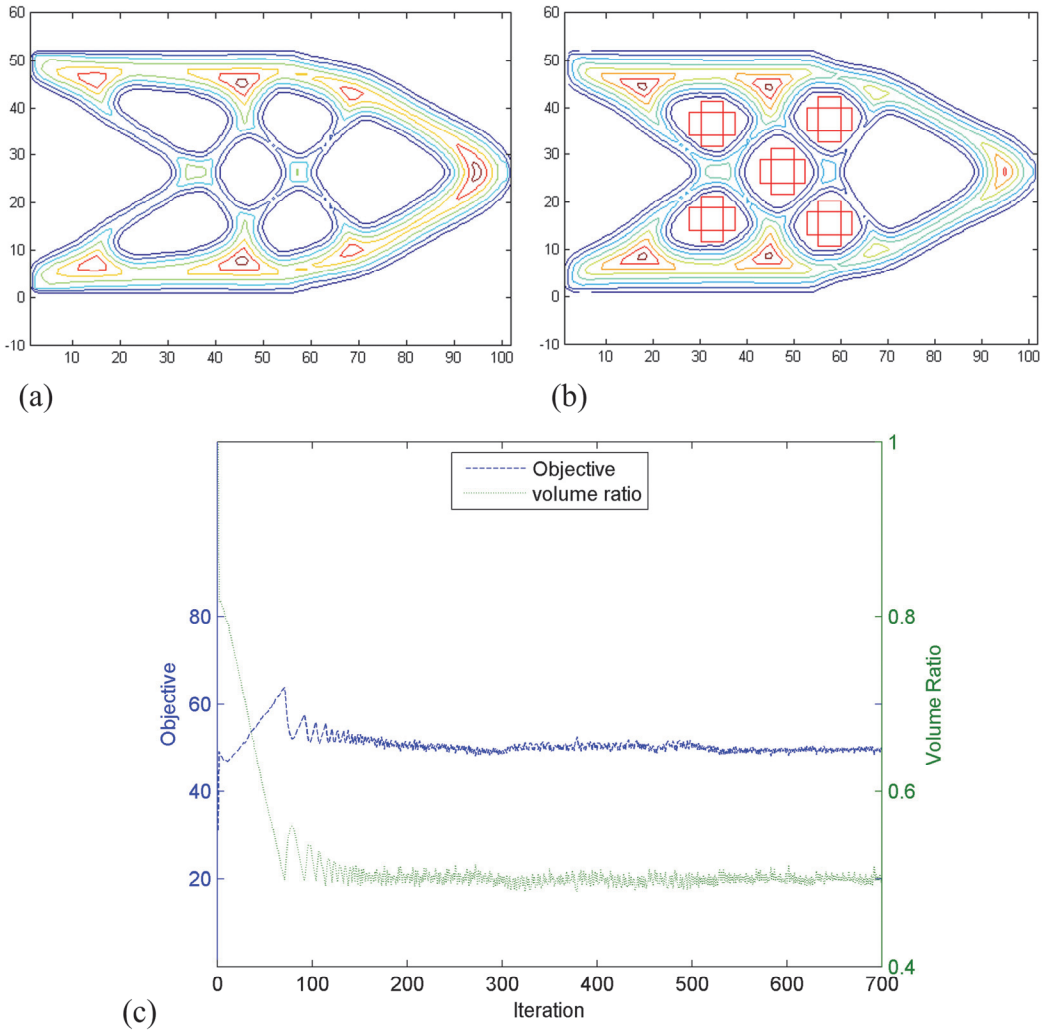

Figure 15. The optimization result subjected to the cross void feature control of size L=10 and H=4 for each rectangle bar (compliance = 49.41) (a) Optimization result of the auxiliary algorithm ($K_1 = 5$); (b) The final optimization result; (c) The overall convergence history

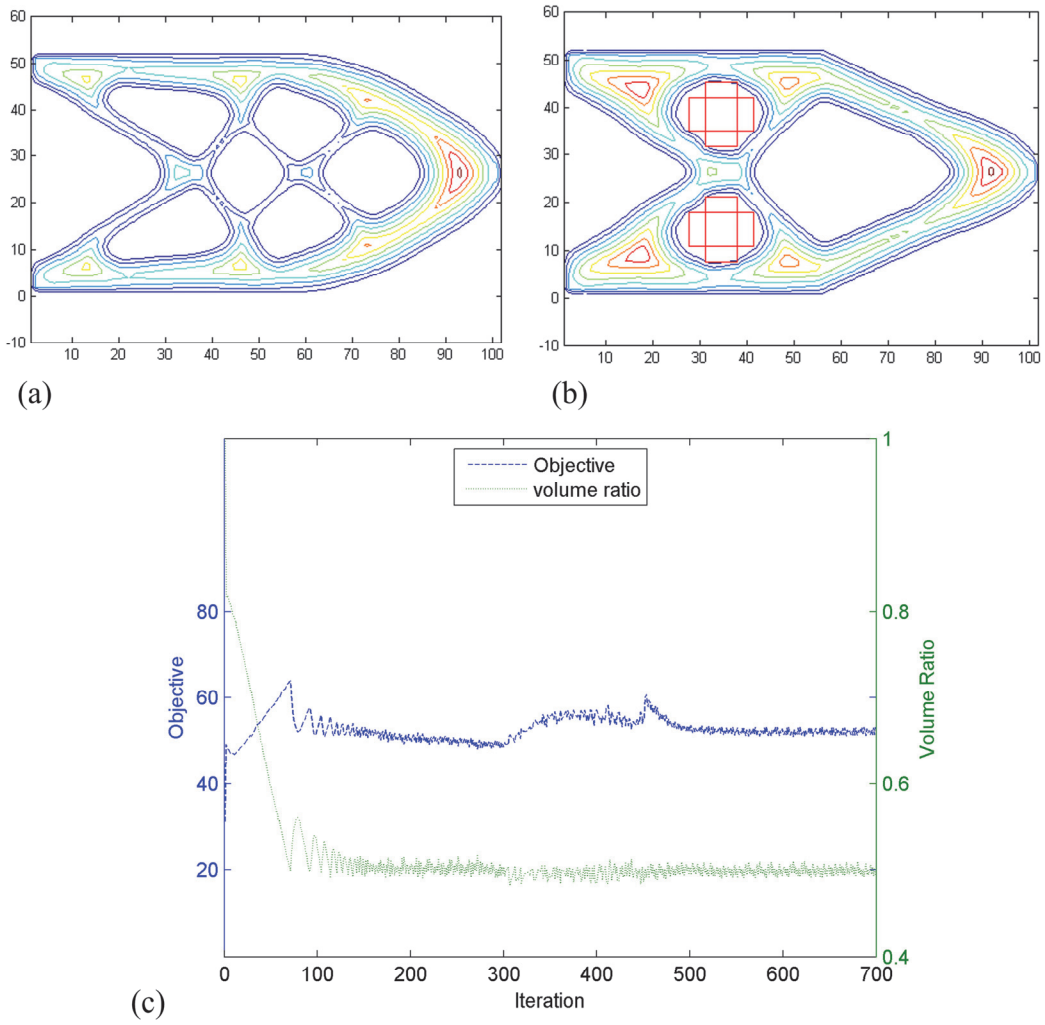

Figure 16. The optimization result subjected to the cross void feature control of size L=14 and H=6 for each rectangle bar (compliance = 51.40) (a) Optimization result of the auxiliary algorithm ($K_1 = 6$); (b) The final optimization result; (c) The overall convergence history

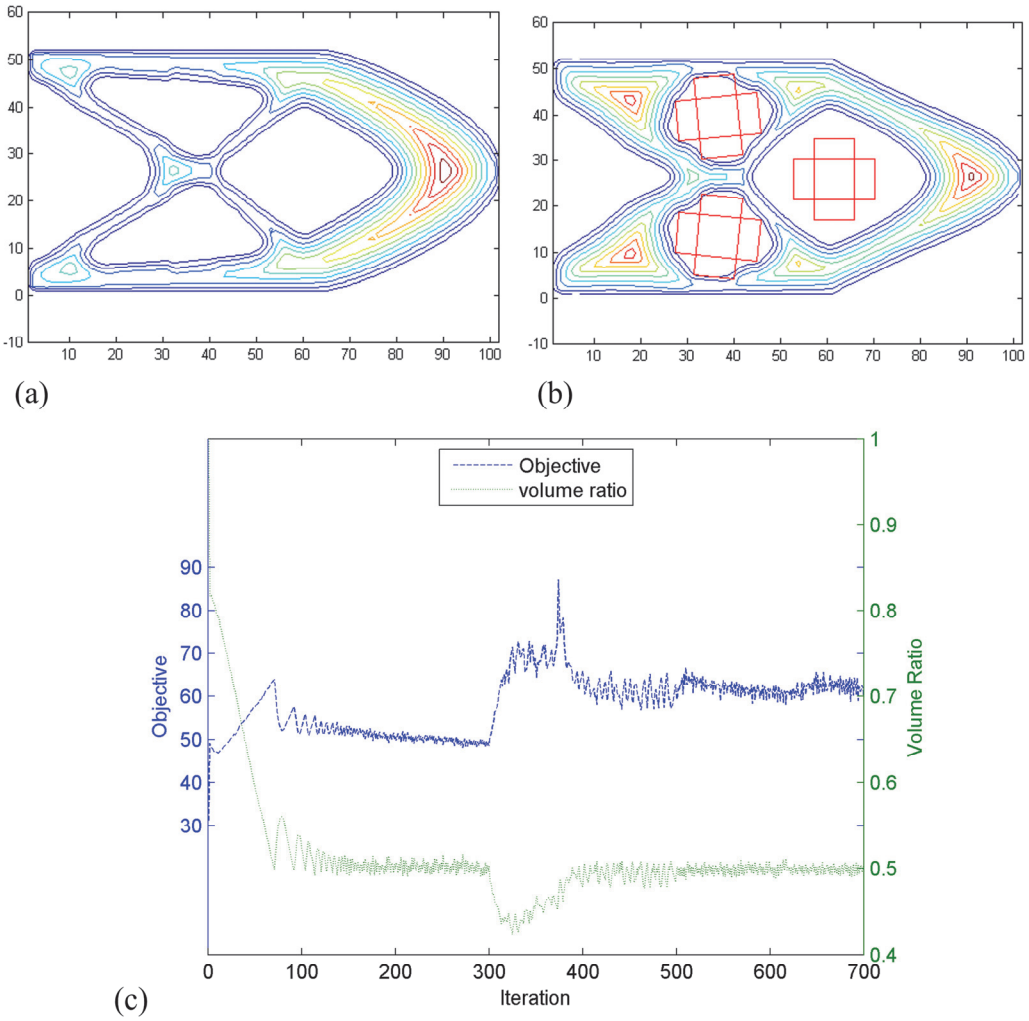

Figure 17. The optimization result subjected to the cross void feature control of size L=18 and H=8 for each rectangle bar (compliance = 61.96) (a) Optimization result of the auxiliary algorithm ($K_1 = 7$); (b) The final optimization result; (c) The overall convergence history

The last example is the MBB structure problem. As shown in Fig. 18, the two bottom corners are vertically fixed and a vertical unit force is loaded at the middle of the top edge. The objective is to minimize the structural compliance under the maximum material volume fraction of 0.5. The same material properties used by the earlier examples are employed.

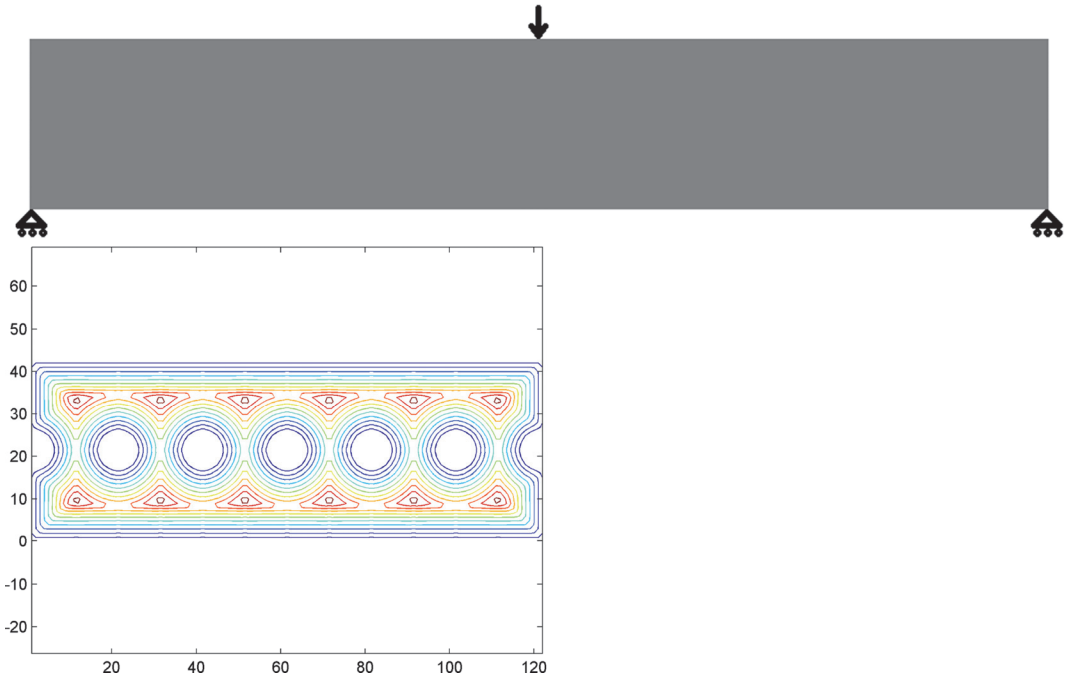

Figure 18. The MBB structure problem (240*40)

The intermediate and final optimization results subjected to different cross void feature sizes are shown in Fig. (19-20). And the intermediate and final optimization results subjected to different T-shaped void feature sizes are demonstrated in Fig. (21-22). It is worth noticing that, only the left half of the MBB structure is demonstrated in the results because of the symmetry.

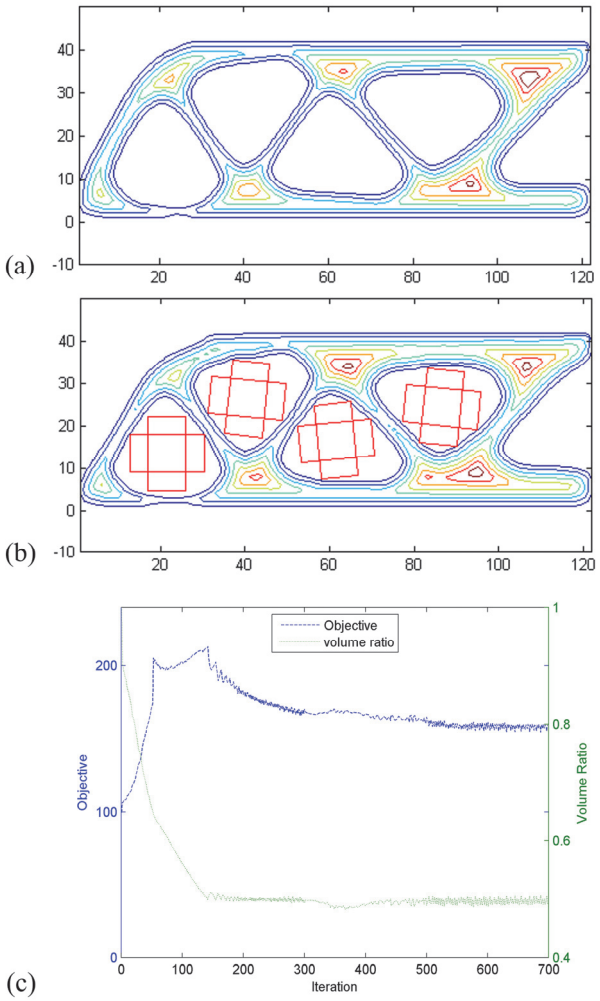

Figure 19. The optimization result subjected to the cross void feature control of size L=18 and H=8 for each rectangle bar (compliance = 157.88) (a) Optimization result of the auxiliary algorithm ($K_1 = 9.5$); (b) The final optimization result; (c) The overall convergence history

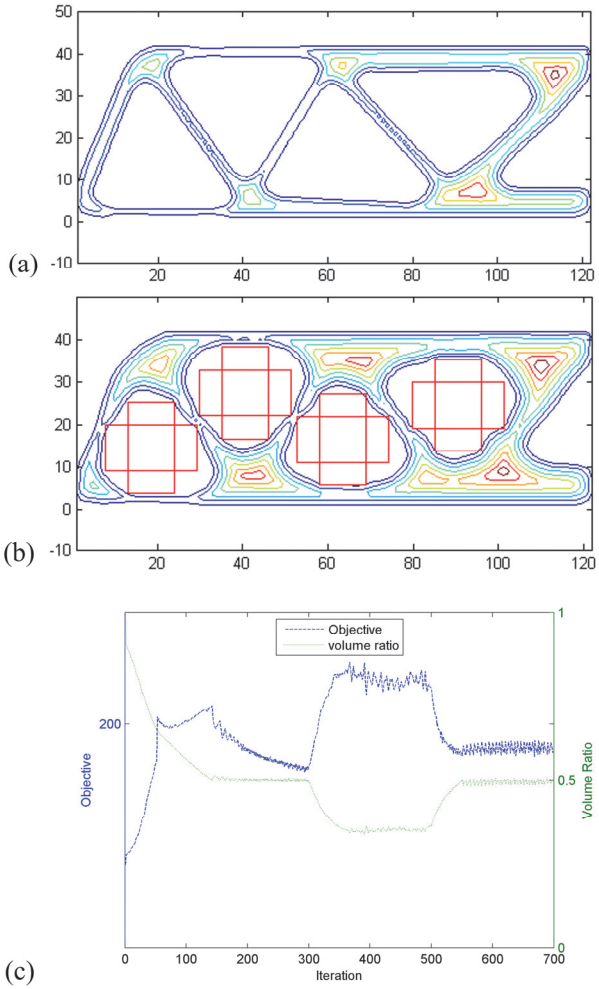

Figure 20. The optimization result subjected to the cross void feature control of size L=22 and H=10 for each rectangle bar (compliance = 179.69) (a) Optimization result of the auxiliary algorithm ($K_1 = 11$); (b) The final optimization result; (c) The overall convergence history

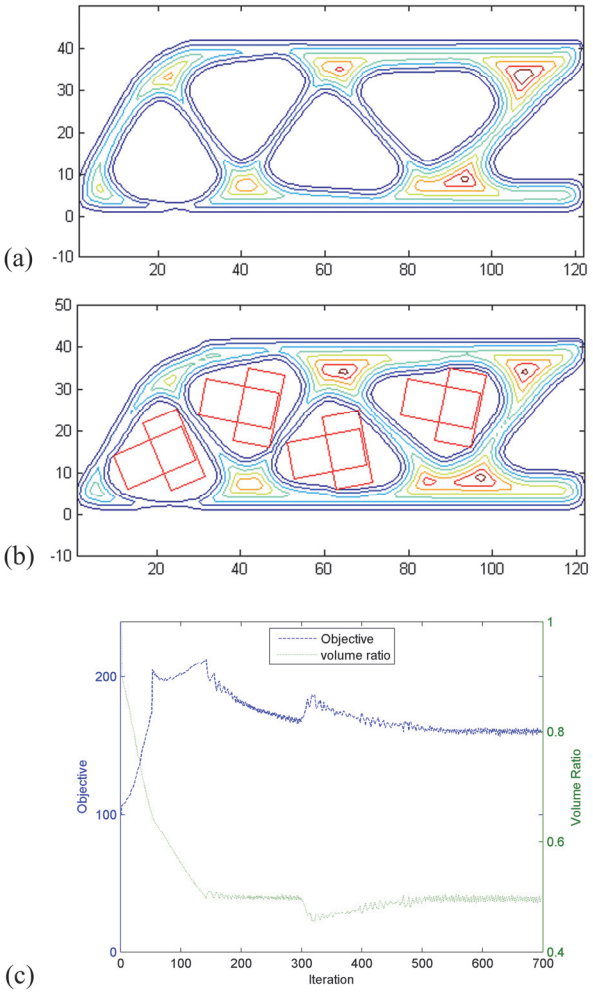

Figure 21. The optimization result subjected to the T-shape void feature control of size L=18 and H=8 for each rectangle bar (compliance = 159.23) (a) Optimization result of the auxiliary algorithm ($K_1 = 9.5$); (b) The final optimization result; (c) The overall convergence history

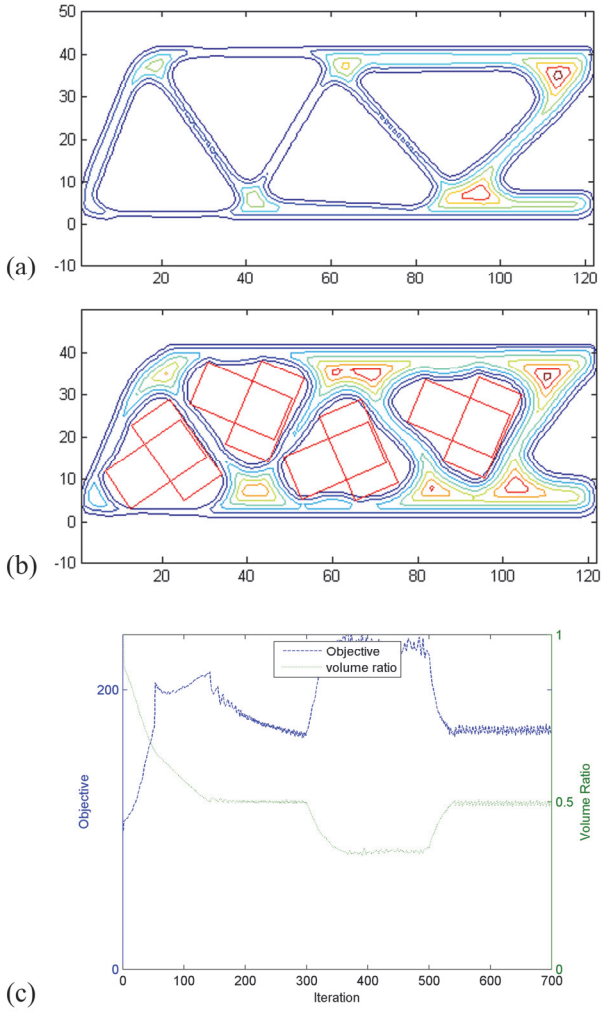

Figure 22. The optimization result subjected to the T-shape void feature control of size L=22 and H=10 for each rectangle bar (compliance = 169.73) (a) Optimization result of the auxiliary algorithm ($K_1 = 11$); (b) The final optimization result; (c) The overall convergence history

In summary of the numerical examples studied in this section, the following observations can be made: (i) The void feature control effect is satisfactory even in the case of large void feature candidates; and (ii) larger void feature generally leads to more compromise of the structural performance.

In addition, it is worth a discussion about the convergence history, which is divided into three stages including the unconstrained optimization, the auxiliary optimization, and the void feature-constrained optimization. The unconstrained optimization indicates that for the first *N* iterations (*N* equals to 200 or 300 for the numerical examples in this section), no additional constraints are employed, which evolves the structure approaching the optimal topology. Then, the auxiliary optimization enlarges the interior voids to ensure stability of the void feature control; however, the structural performance is generally compromised. Finally, the void feature-constrained optimization converges the result to the optimum, where satisfactory void feature control effect could be achieved.

6. Conclusion

In summary, this paper presents a void feature control method. The algorithm takes extra control of the boundary evolution of the interior voids, to guarantee that the specified void feature (could be in any geometric form) is well contained by each of the interior voids in the final topological design. In addition, an auxiliary algorithm has been developed to enhance the numerical implementation stability, by enlarging the interior void areas. This method has been proven effective by a list of numerical examples.

Specifically about the numerical implementation, the convergence process has been carefully controlled by different strategies. It is firstly solved as an unconstrained problem, which drives the structure approaching the optimal topology; then, the auxiliary algorithm enlarges the interior voids as a preparation step of the void feature control; finally, the void feature control constraints are solved to derive the optimal topology design with satisfactory control effect.

A unique characteristic of this method is that, quantity of the void features does not need to be pre-specified; instead, it is tightly bonded to the topology evolution process. In the future work, we intend to further develop this void feature control method, targeting that, not only the quantity need not to be specified, but also the void feature types should not be pre-determined. Potentially, this target can be realized by introducing combined feature representations.

Acknowledgement

The authors would like to acknowledge the support from China Scholarship Council (CSC) and the National Science Foundation (CMMI-1634261).

Reference

[1] M.P. Bendsøe, O. Sigmund, Topology Optimization, Springer Berlin Heidelberg, Berlin, Heidelberg, 2004. http://link.springer.com/10.1007/978-3-662-05086-6 (accessed May 26, 2016).

[2] M.P. Bendsøe, Optimal shape design as a material distribution problem, Struct. Optim. 1 (1989) 193–202. doi:10.1007/BF01650949.

[3] Y.M. Xie, G.P. Steven, A simple evolutionary procedure for structural optimization, Comput. Struct. 49 (1993) 885–896. doi:10.1016/0045-7949(93)90035-C.

[4] G. Allaire, F. Jouve, A.-M. Toader, Structural optimization using sensitivity analysis and a level-set method, J. Comput. Phys. 194 (2004) 363–393. doi:10.1016/j.jcp.2003.09.032.

[5] M.Y. Wang, X. Wang, D. Guo, A level set method for structural topology optimization, Comput. Methods Appl. Mech. Eng. 192 (2003) 227–246. doi:10.1016/S0045-7825(02)00559-5.

[6] M.P. Bendsøe, N. Kikuchi, Generating optimal topologies in structural design using a homogenization method, Comput. Methods Appl. Mech. Eng. 71 (1988) 197–224. doi:10.1016/0045-7825(88)90086-2.

[7] T. Borrvall, J. Petersson, Topology optimization of fluids in Stokes flow, Int. J. Numer. Methods Fluids. 41 (2003) 77–107. doi:10.1002/fld.426.
[8] S. Zhou, Q. Li, A variational level set method for the topology optimization of steady-state Navier–Stokes flow, J. Comput. Phys. 227 (2008) 10178–10195. doi:10.1016/j.jcp.2008.08.022.
[9] G.P. Steven, Q. Li, Y.M. Xie, Evolutionary topology and shape design for general physical field problems, Comput. Mech. 26 (2000) 129–139. doi:10.1007/s004660000160.
[10] A. Gersborg-Hansen, O. Sigmund, R.B. Haber, Topology optimization of channel flow problems, Struct. Multidiscip. Optim. 30 (2005) 181–192. doi:10.1007/s00158-004-0508-7.
[11] S.-H. Ha, S. Cho, Topological Shape Optimization of Heat Conduction Problems using Level Set Approach, Numer. Heat Transf. Part B Fundam. 48 (2005) 67–88. doi:10.1080/10407790590935966.
[12] T. Yamada, K. Izui, S. Nishiwaki, A Level Set-Based Topology Optimization Method for Maximizing Thermal Diffusivity in Problems Including Design-Dependent Effects, J. Mech. Des. 133 (2011) 031011–031011. doi:10.1115/1.4003684.
[13] C. Zhuang, Z. Xiong, H. Ding, A level set method for topology optimization of heat conduction problem under multiple load cases, Comput. Methods Appl. Mech. Eng. 196 (2007) 1074–1084. doi:10.1016/j.cma.2006.08.005.
[14] Q. Li, G.P. Steven, O.M. Querin, Y.M. Xie, Shape and topology design for heat conduction by Evolutionary Structural Optimization, Int. J. Heat Mass Transf. 42 (1999) 3361–3371. doi:10.1016/S0017-9310(99)00008-3.
[15] N.P. van Dijk, K. Maute, M. Langelaar, F. van Keulen, Level-set methods for structural topology optimization: a review, Struct. Multidiscip. Optim. 48 (2013) 437–472. doi:10.1007/s00158-013-0912-y.
[16] G.I.N. Rozvany, A critical review of established methods of structural topology optimization, Struct. Multidiscip. Optim. 37 (2009) 217–237. doi:10.1007/s00158-007-0217-0.
[17] O. Sigmund, K. Maute, Topology optimization approaches, Struct. Multidiscip. Optim. 48 (2013) 1031–1055. doi:10.1007/s00158-013-0978-6.
[18] J. Liu, Y. Ma, A survey of manufacturing oriented topology optimization methods, Adv. Eng. Softw. 100 (2016) 161–175. doi:10.1016/j.advengsoft.2016.07.017.
[19] D.J. Munk, G.A. Vio, G.P. Steven, Topology and shape optimization methods using evolutionary algorithms: a review, Struct. Multidiscip. Optim. 52 (2015) 613–631. doi:10.1007/s00158-015-1261-9.
[20] J.D. Deaton, R.V. Grandhi, A survey of structural and multidisciplinary continuum topology optimization: post 2000, Struct. Multidiscip. Optim. 49 (2014) 1–38. doi:10.1007/s00158-013-0956-z.
[21] W. Zhang, L. Xia, J. Zhu, Q. Zhang, Some Recent Advances in the Integrated Layout Design of Multicomponent Systems, J. Mech. Des. 133 (2011) 104503–104503. doi:10.1115/1.4005083.
[22] Z. Qian, G.K. Ananthasuresh, Optimal Embedding of Rigid Objects in the Topology Design of Structures, Mech. Based Des. Struct. Mach. 32 (2004) 165–193. doi:10.1081/SME-120030555.
[23] J. Zhu, W. Zhang, P. Beckers, Y. Chen, Z. Guo, Simultaneous design of components layout and supporting structures using coupled shape and topology optimization technique, Struct. Multidiscip. Optim. 36 (2008) 29–41. doi:10.1007/s00158-007-0155-x.
[24] J. Liu, Y.-S. Ma, 3D level-set topology optimization: a machining feature-based approach, Struct. Multidiscip. Optim. 52 (2015) 563–582. doi:10.1007/s00158-015-1263-7.
[25] Y. Mei, X. Wang, G. Cheng, A feature-based topological optimization for structure design, Adv. Eng. Softw. 39 (2008) 71–87. doi:10.1016/j.advengsoft.2007.01.023.
[26] B.S. Lazarov, F. Wang, O. Sigmund, Length scale and manufacturability in density-based topology optimization, Arch. Appl. Mech. 86 (2016) 189–218. doi:10.1007/s00419-015-1106-4.
[27] J.K. Guest, Topology optimization with multiple phase projection, Comput. Methods Appl. Mech. Eng. 199 (2009) 123–135. doi:10.1016/j.cma.2009.09.023.

[28] J.K. Guest, Imposing maximum length scale in topology optimization, Struct. Multidiscip. Optim. 37 (2009) 463–473. doi:10.1007/s00158-008-0250-7.
[29] J.K. Guest, J.H. Prévost, T. Belytschko, Achieving minimum length scale in topology optimization using nodal design variables and projection functions, Int. J. Numer. Methods Eng. 61 (2004) 238–254. doi:10.1002/nme.1064.
[30] T.A. Poulsen, A new scheme for imposing a minimum length scale in topology optimization, Int. J. Numer. Methods Eng. 57 (2003) 741–760. doi:10.1002/nme.694.
[31] M. Schevenels, B.S. Lazarov, O. Sigmund, Robust topology optimization accounting for spatially varying manufacturing errors, Comput. Methods Appl. Mech. Eng. 200 (2011) 3613–3627. doi:10.1016/j.cma.2011.08.006.
[32] O. Sigmund, Manufacturing tolerant topology optimization, Acta Mech. Sin. 25 (2009) 227–239. doi:10.1007/s10409-009-0240-z.
[33] O. Sigmund, Morphology-based black and white filters for topology optimization, Struct. Multidiscip. Optim. 33 (2007) 401–424. doi:10.1007/s00158-006-0087-x.
[34] F. Wang, B.S. Lazarov, O. Sigmund, On projection methods, convergence and robust formulations in topology optimization, Struct. Multidiscip. Optim. 43 (2011) 767–784. doi:10.1007/s00158-010-0602-y.
[35] W. Zhang, W. Zhong, X. Guo, An explicit length scale control approach in SIMP-based topology optimization, Comput. Methods Appl. Mech. Eng. 282 (2014) 71–86. doi:10.1016/j.cma.2014.08.027.
[36] M. Zhou, B.S. Lazarov, F. Wang, O. Sigmund, Minimum length scale in topology optimization by geometric constraints, Comput. Methods Appl. Mech. Eng. 293 (2015) 266–282. doi:10.1016/j.cma.2015.05.003.
[37] G. Allaire, F. Jouve, G. Michailidis, Thickness control in structural optimization via a level set method, Struct. Multidiscip. Optim. 53 (2016) 1349–1382. doi:10.1007/s00158-016-1453-y.
[38] S. Chen, M.Y. Wang, A.Q. Liu, Shape feature control in structural topology optimization, Comput.-Aided Des. 40 (2008) 951–962. doi:10.1016/j.cad.2008.07.004.
[39] X. Guo, W. Zhang, W. Zhong, Explicit feature control in structural topology optimization via level set method, Comput. Methods Appl. Mech. Eng. 272 (2014) 354–378. doi:10.1016/j.cma.2014.01.010.
[40] J. Liu, Y. Ma, J. Fu, K. Duke, A novel CACD/CAD/CAE integrated design framework for fiber-reinforced plastic parts, Adv. Eng. Softw. 87 (2015) 13–29. doi:10.1016/j.advengsoft.2015.04.013.
[41] J. Luo, Z. Luo, S. Chen, L. Tong, M.Y. Wang, A new level set method for systematic design of hinge-free compliant mechanisms, Comput. Methods Appl. Mech. Eng. 198 (2008) 318–331. doi:10.1016/j.cma.2008.08.003.
[42] Q. Xia, T. Shi, Constraints of distance from boundary to skeleton: For the control of length scale in level set based structural topology optimization, Comput. Methods Appl. Mech. Eng. 295 (2015) 525–542. doi:10.1016/j.cma.2015.07.015.
[43] J. Liu, H. Yu, Y. Ma, Minimum void length scale control in level set topology optimization subject to machining radii, Comput.-Aided Des. 81 (2016) 70–80. doi:10.1016/j.cad.2016.09.007.
[44] Y. Wang, L. Zhang, M.Y. Wang, Length scale control for structural optimization by level sets, Comput. Methods Appl. Mech. Eng. 305 (2016) 891–909. doi:10.1016/j.cma.2016.03.037.
[45] R.B. Haber, C.S. Jog, M.P. Bendsøe, A new approach to variable-topology shape design using a constraint on perimeter, Struct. Optim. 11 (1996) 1–12. doi:10.1007/BF01279647.
[46] B. Bourdin, A. Chambolle, Design-dependent loads in topology optimization, ESAIM Control Optim. Calc. Var. 9 (2003) 19–48. doi:10.1051/cocv:2002070.
[47] A. Takezawa, S. Nishiwaki, M. Kitamura, Shape and topology optimization based on the phase field method and sensitivity analysis, J. Comput. Phys. 229 (2010) 2697–2718. doi:10.1016/j.jcp.2009.12.017.

[48] L. Xia, J. Zhu, W. Zhang, P. Breitkopf, An implicit model for the integrated optimization of component layout and structure topology, Comput. Methods Appl. Mech. Eng. 257 (2013) 87–102. doi:10.1016/j.cma.2013.01.008.
[49] J. Zhang, W.H. Zhang, J.H. Zhu, L. Xia, Integrated layout design of multi-component systems using XFEM and analytical sensitivity analysis, Comput. Methods Appl. Mech. Eng. 245–246 (2012) 75–89. doi:10.1016/j.cma.2012.06.022.
[50] Z. Kang, Y. Wang, Integrated topology optimization with embedded movable holes based on combined description by material density and level sets, Comput. Methods Appl. Mech. Eng. 255 (2013) 1–13. doi:10.1016/j.cma.2012.11.006.
[51] H.-H. Gao, J.-H. Zhu, W.-H. Zhang, Y. Zhou, An improved adaptive constraint aggregation for integrated layout and topology optimization, Comput. Methods Appl. Mech. Eng. 289 (2015) 387–408. doi:10.1016/j.cma.2015.02.022.
[52] W. Zhang, W. Zhong, X. Guo, Explicit layout control in optimal design of structural systems with multiple embedding components, Comput. Methods Appl. Mech. Eng. 290 (2015) 290–313. doi:10.1016/j.cma.2015.03.007.
[53] Z. Kang, Y. Wang, Y. Wang, Structural topology optimization with minimum distance control of multiphase embedded components by level set method, Comput. Methods Appl. Mech. Eng. 306 (2016) 299–318. doi:10.1016/j.cma.2016.04.001.
[54] S.R.M. Almeida, G.H. Paulino, E.C.N. Silva, A simple and effective inverse projection scheme for void distribution control in topology optimization, Struct. Multidiscip. Optim. 39 (2009) 359–371. doi:10.1007/s00158-008-0332-6.
[55] S.-H. Ha, J.K. Guest, Optimizing inclusion shapes and patterns in periodic materials using Discrete Object Projection, Struct. Multidiscip. Optim. 50 (2014) 65–80. doi:10.1007/s00158-013-1026-2.
[56] J.K. Guest, Optimizing the layout of discrete objects in structures and materials: A projection-based topology optimization approach, Comput. Methods Appl. Mech. Eng. 283 (2015) 330–351. doi:10.1016/j.cma.2014.09.006.
[57] J.A. Norato, B.K. Bell, D.A. Tortorelli, A geometry projection method for continuum-based topology optimization with discrete elements, Comput. Methods Appl. Mech. Eng. 293 (2015) 306–327. doi:10.1016/j.cma.2015.05.005.
[58] X. Guo, W. Zhang, W. Zhong, Doing Topology Optimization Explicitly and Geometrically—A New Moving Morphable Components Based Framework, J. Appl. Mech. 81 (2014) 081009–081009. doi:10.1115/1.4027609.
[59] G. Cheng, Y. Mei, X. Wang, A Feature-Based Structural Topology Optimization Method, in: M.P. Bendsøe, N. Olhoff, O. Sigmund (Eds.), IUTAM Symp. Topol. Des. Optim. Struct. Mach. Mater., Springer Netherlands, 2006: pp. 505–514. doi:10.1007/1-4020-4752-5_48.
[60] J. Chen, V. Shapiro, K. Suresh, I. Tsukanov, Shape optimization with topological changes and parametric control, Int. J. Numer. Methods Eng. 71 (2007) 313–346. doi:10.1002/nme.1943.
[61] S.H. Gopalakrishnan, K. Suresh, Feature sensitivity: A generalization of topological sensitivity, Finite Elem. Anal. Des. 44 (2008) 696–704. doi:10.1016/j.finel.2008.03.006.
[62] M. Zhou, M.Y. Wang, Engineering feature design for level set based structural optimization, Comput.-Aided Des. 45 (2013) 1524–1537. doi:10.1016/j.cad.2013.06.016.
[63] W. Zhang, J. Yuan, J. Zhang, X. Guo, A new topology optimization approach based on Moving Morphable Components (MMC) and the ersatz material model, Struct. Multidiscip. Optim. 53 (2016) 1243–1260. doi:10.1007/s00158-015-1372-3.
[64] X. Guo, W. Zhang, J. Zhang, J. Yuan, Explicit structural topology optimization based on moving morphable components (MMC) with curved skeletons, Comput. Methods Appl. Mech. Eng. 310 (2016) 711–748. doi:10.1016/j.cma.2016.07.018.
[65] Y. Zhou, W. Zhang, J. Zhu, Z. Xu, Feature-driven topology optimization method with signed distance function, Comput. Methods Appl. Mech. Eng. 310 (2016) 1–32. doi:10.1016/j.cma.2016.06.027.

[66] Q. Xia, M.Y. Wang, Simultaneous optimization of the material properties and the topology of functionally graded structures, Comput.-Aided Des. 40 (2008) 660–675. doi:10.1016/j.cad.2008.01.014.
[67] S. Osher, J.A. Sethian, Fronts propagating with curvature-dependent speed: Algorithms based on Hamilton-Jacobi formulations, J. Comput. Phys. 79 (1988) 12–49. doi:10.1016/0021-9991(88)90002-2.